Magnetic Maps and Models for Alternative Navigation

Rick Saltus
CIRES/NOAA
University of Colorado
Boulder, Colorado USA
richard.saltus@colorado.edu

Patrick Alken
CIRES/NOAA
University of Colorado
Boulder, Colorado

Annette Balmes
CIRES/NOAA
University of Colorado
Boulder, Colorado

Nir Boneh
CIRES/NOAA
University of Colorado
Boulder, Colorado

Sam Califf
CIRES/NOAA
University of Colorado
Boulder, Colorado

Arnaud Chulliat
CIRES/NOAA
University of Colorado
Boulder, Colorado

Brian Meyer
NOAA
David Skaggs Research Center
Boulder, Colorado

Manoj Nair
CIRES/NOAA
University of Colorado
Boulder, Colorado

***Abstract*— Magnetic navigation requires the comparison of onboard magnetic sensor measurements to reference magnetic maps and models. Magnetic maps and models are available at a wide range of scales and scope. At any given location, measurements of the ambient magnetic field are the sum of various components, including sources internal and external to the Earth. This paper discusses maps and models of the internal components sourced in the core and lithosphere of the Earth. The long-wavelength, slowly-time-varying core field of the Earth is represented by global, satellite-based models. The time-invariant lithospheric magnetic field is represented at its longest wavelengths by spherical harmonic models based on data from the CHAMP and SWARM satellite missions and at resolutions smaller than ~300 km by grid products based on the processing of airborne, marine, and ground surveys. Regional to local magnetic anomaly maps and grids are available for selected areas at resolutions down to 100 m. Evaluation of possible map/model performance for a given magnetic navigation scenario requires consideration of amplitude and frequency of magnetic field variations, and magnetic map/model uncertainty. We present a basic analysis of magnetic navigation signals as a function of altitude and velocity.**

Keywords—magnetic field, navigation, maps, models

I. Introduction

The Earth's magnetic field is a dynamic system consisting of multiple sources with both long and short-wavelength variability in both time and space (Table 1). The total magnetic field measured by a physical sensor is the sum of these sources.

Internal magnetic field sources are those originating from processes and magnetic property variations at the Earth's surface and below. The core field is smoothly varying at the Earth's surface and ranges in amplitude from around 20,000 nT (at low latitudes) to around 60,000 nT (at high latitudes). Fig. 1 shows the intensity of the core (main) field as depicted by the 2020 World Magnetic Model [1].

TABLE I. Informal Breakdown of Primary Magnetic Sources

	Amplitude (nT OM)	Time scale	Nav status
Internal			
Core	50,000	years	models
Lithosphere	100's	eons	maps
Cultural	100's	days/years	unmapped noise
External			
High Lat	>100's	hours	poorly modeled noise
Mid Lat	10's	daily	partially modeled noise
Low Lat	10's	daily	partially modeled noise

Rocks containing magnetic minerals in the crust and parts of the upper mantle cause magnetic field variations, termed the *lithospheric field*. Lithospheric magnetic field variations are called *magnetic anomalies*. These anomalies are the part of the Earth's magnetic field that is commonly shown on magnetic maps. The patterns on magnetic anomaly maps can be analyzed for geologic and tectonic studies. Exploration/analysis use cases are the primary motivation for magnetic maps.

The North America Magnetic Anomaly Grid (NAMAG) is an example of a regional magnetic anomaly grid [2]. Magnetic minerals in the Earth's crust (and portions of the upper mantle) cause anomalies through two physical processes: *Induced* magnetic anomalies result from interaction of magnetic minerals with the ambient core field. As the core field changes in time, so too will this part of the lithospheric field; *Remanent* magnetic anomalies are static relative to the core field. The temporal

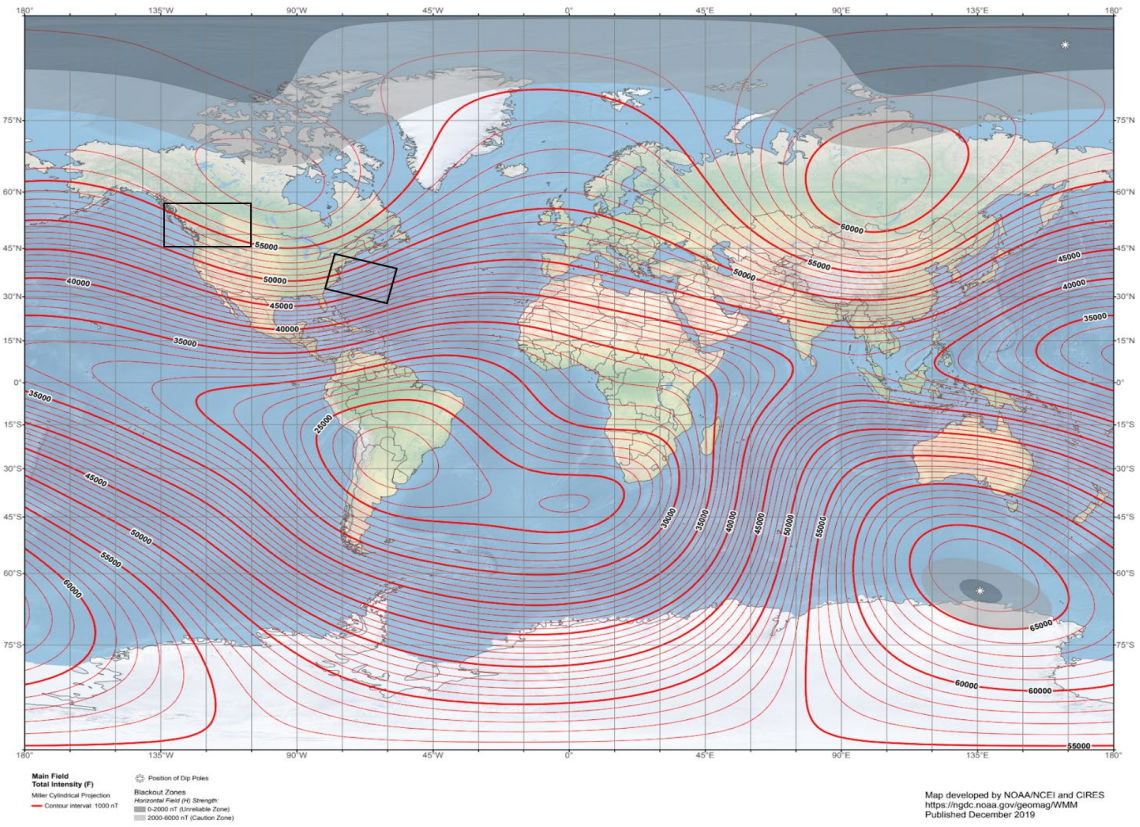

Fig. 1. World Magnetic Model 2020. Contours show isolines of (scalar) total field. The approximate location of the detailed maps in Fig. 9C are shown by the black boxes. A full suite of maps is available at https://www.ncei.noaa.gov/products/world-magnetic-model.

variations of the induced anomalies are generally ignored in map compilations, but there are certain special cases (at high latitudes) where these changes could affect the use of vintage magnetic anomaly data and maps for modern navigation [3].

Fig. 2 shows the lithospheric anomaly field as depicted by EMAG2v3 [4], [5]. Globally the lithospheric magnetic anomalies at 4 km altitude (e.g., EMAG2v3) generally vary between -200 and +200 nT with a standard deviation of about 100 nT. At sea level, the global lithospheric magnetic anomalies over ocean regions have the same roughly +- 200 nT distribution with a lower standard deviation of about 70 nT.

Human infrastructure includes magnetic materials or the generation of changing electric fields that create magnetic disturbances. Some of these *cultural* variations are relatively static and could, in theory, be mapped. However, maps of these field disturbances are not generally available. Other cultural magnetic field variations are dynamic and represent a source of uncertainty for near surface magnetic navigation, particularly in urban areas.

The Earth is pummeled constantly by the solar wind. The variability in the intensity of the solar wind and its interaction with the outer portions of the Earth's internal field, causes time varying disturbances for in situ measurement of the total magnetic field.

Electric currents flowing in the conducting layers of the Earth's ionosphere generate additional magnetic field disturbances. Some components of this time-varying signal can be predicted, particularly at mid and low latitudes, and can be partially removed using dedicated global or regional models, thus improving the signal to noise ratio of the static magnetic field used for navigation. However, these external fields, particularly during periods of extreme "space weather", are unpredictable in detail. While the understanding of these variations is important for magnetic navigation, they are not the primary focus of this paper.

II. Map and Model Overview

The long-wavelength, slowly time-varying core field of the Earth is represented by global, satellite-based models such as the International Geomagnetic Reference Field (IGRF; [6]) and the World Magnetic Model [1]. See Fig. 1 for a map depiction of the WMM 2020 model of the core field. The core field dominates the magnetic frequency spectrum to spherical harmonic degree 15 (spatial scale of ~2600 km; Table 2).

The CHAOS magnetic field model [9] covers the static core field (spherical harmonics <=15), the very large-scale crustal field (up to spherical harmonics ~<25) as well as the time variations of secular variation (for spherical harmonics<=20). The static part of the CHAOS model for spherical harmonics >25 is the same as LCS-1 (discussed below).

The lithospheric magnetic field is represented at its longest wavelengths by spherical harmonic models such as MF7 (based on data from the CHAMP satellite mission; [7]) and LCS-1

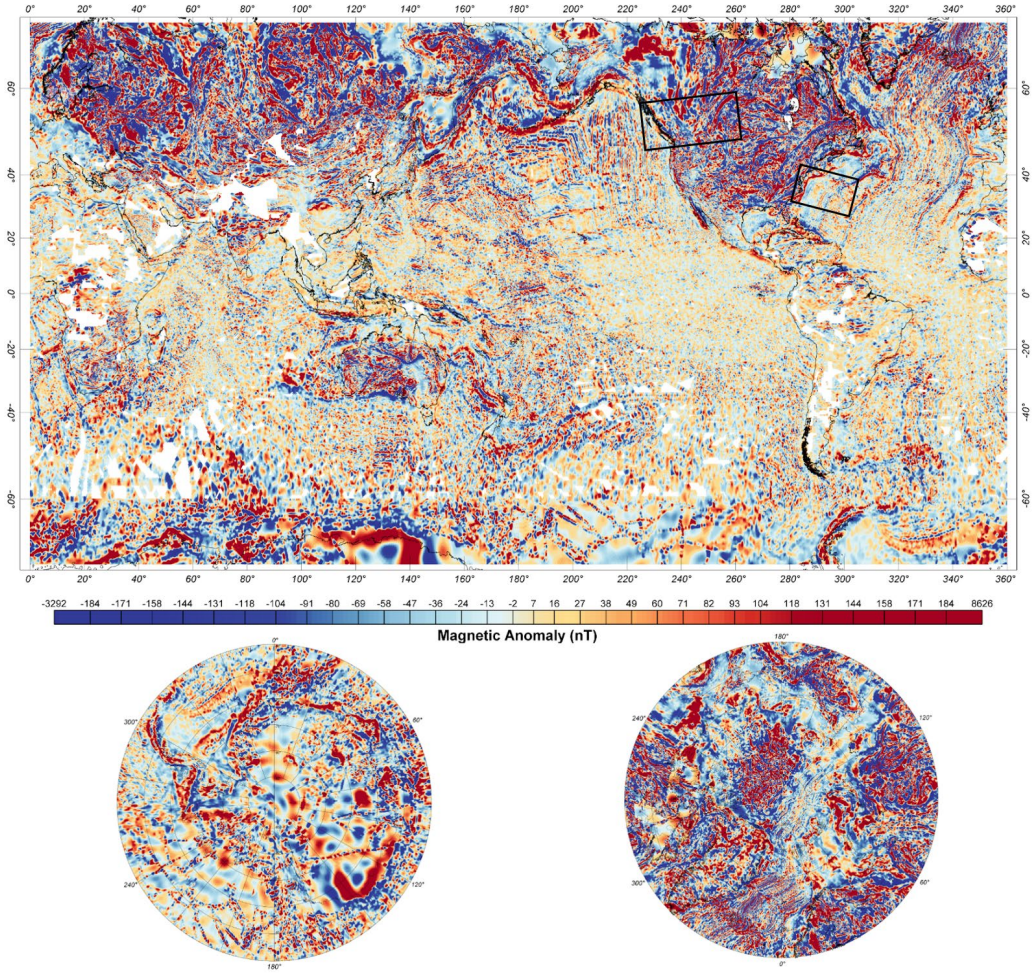

Fig. 2. Lithospheric anomaly field as depicted by EMAG2v3 [5]. The approximate location of the maps shown in Fig. 9C are shown by the black boxes.

(based on data from both the CHAMP and SWARM missions; [8]). These long-wavelength lithospheric models extend to spherical harmonic degree and order of 133 (MF7) and 166 (LCS-1), corresponding to spatial scales of ~300 and ~240 km, respectively.

At spatial resolutions smaller than ~300 km, lithospheric magnetic compilations are generally grid (map) products. Several global compilations to ~4 km resolution are available (e.g., EMAG2 and WDMAM). The uncertainty in these global high-resolution compilations is highly variable, especially in the marine regions. For shorter wavelengths, regional to local magnetic anomaly maps and are available from national geological surveys, academia, or the exploration sector. Much of this information is publicly available, but some is proprietary.

Several hybrid models that combine satellite and survey-based data are included in Table 2. These models include the commercial HDGM and BGGM as well as the EMM research model. Wavelengths shorter than 300 km in these models come from spherical

TABLE II. SUMMARY TABLE FOR SPATIAL FREQUENCY CONTENT OF WIDELY DISTRIBUTED GLOBAL MAGNETIC FIELD MODELS.

Magnetic model resolution in spherical harmonics and distance (at the equator)					
Global model or grid	Scale range of models: light gray = sat data dark gray = survey data		Spherical Harmonic degree and order	Distance	
				kilometers	degrees	minutes
		CORE	2	16012.1	180.00	10800.0
			8	4709.4	45.00	2700.0
WMM			12	3202.4	30.00	1800.0
IGRF			13	2965.2	27.69	1661.5
			15	2582.6	24.00	1440.0
			20	1952.7	18.00	1080.0
CHAOS			50	792.7	7.20	432.0
			100	398.3	3.60	216.0
MF7			133	299.9	2.71	162.4
LCS-1		LITHOSPHERE	166	240.4	2.17	130.1
			300	133.2	1.20	72.0
			500	80.0	0.72	43.2
			750	53.3	0.48	28.8
HDGM, EMM			790	50.6	0.46	27.3
			1000	40.0	0.36	21.6
BGGM			1440	27.8	0.25	15.0
			2000	20.0	0.18	10.8
			3000	13.3	0.12	7.2
			4000	10.0	0.09	5.4
			5000	8.0	0.07	4.3
			7000	5.7	0.05	3.1
WDMAM, EMAG2*			10000	4.0	0.04	2.2
*not spherical harmonic models						

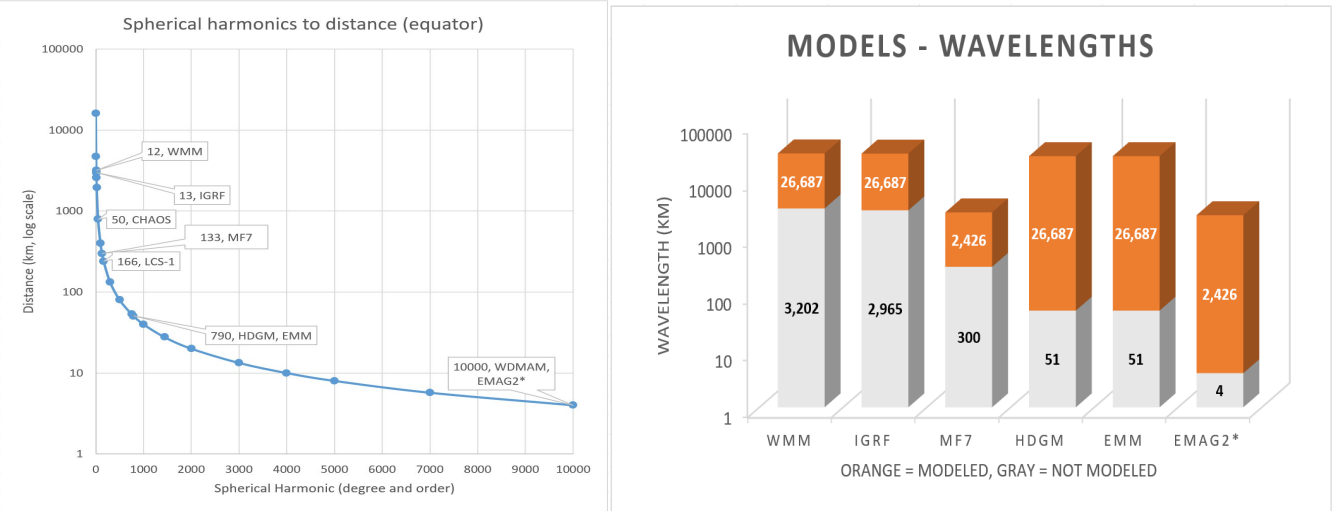

Fig. 3. Graphs showing the relation of spherical harmonic order and degree to spatial scale. (Left) Maximum degree and order for selected models. Distance is plotted on a log scale. (Right) Chart showing spatial scales (in km) for several models.

harmonic representation of the longer wavelengths of global survey models such as EMAG2.

III. Satellite-Based Models

Satellite-based spherical harmonic models of the core field (such as IGRF and WMM) are highly accurate [10], and provide a basis for leveling marine trackline and airborne survey data compilations. These models of the core field consist mathematically of spherical harmonic coefficients, derived from data selection and inversion of satellite data and ground-level measurements [11] (Fig. 3). Spherical harmonic models have a significant operational benefit for use in alternative navigation as field values can be calculated at any position and altitude.

WMM and IGRF are two widely used core field models. WMM is the Department of Defense official main field reference model [1]. It is updated every 5 years, more frequently if the core field is evolving rapidly [12].

IGRF is a research model [6]. It is updated every 5 years. In addition, it is retrospectively revised to form a "definitive" version (DGRF). The IGRF/DGRF models are routinely used in the processing of magnetic survey data to produce lithospheric anomaly maps.

Processing and modeling of satellite data can cover the longest wavelengths of the lithospheric anomaly field. To date the best satellite data for this purpose comes from the end of the CHAMP satellite mission, when the satellite dropped to its lowest orbit before re-entry. MF7 is a model of the longest lithospheric field wavelengths [7]. Models combining CHAMP data with data from the current SWARM mission (e.g., LS-1 [8]) have been constructed to slightly higher resolutions than MF7, but the additional wavelength content has not yet been well verified.

The commercial HDGM [13] and BGGM [14] models, as well as the research EMM model, are spherical harmonic models incorporating a combination of satellite data for core wavelengths and coefficients derived from the longest wavelengths of survey-based grids. The commercial models are used in directional drilling applications.

IV. Survey-Based Maps/Grids

Maps of magnetic anomalies at scales smaller than about 300 km are made using data from aeromagnetic, marine, and ground-based surveys. Fig. 4 illustrates the general process steps for building regional survey-based grids. The most accurate regional maps use data from dedicated modern airborne surveys. Many of the continental regions of the Earth have at least some aeromagnetic data coverage although coverage varies widely. Regional-scale maps of continental regions, such as the NAMAG [2], are constructed by combining individual survey grids. Prior to the publication of the MF7 these compilations do not have reliable long wavelength content. These regional maps are poorly constrained at any wavelengths larger than the mean size of the included surveys.

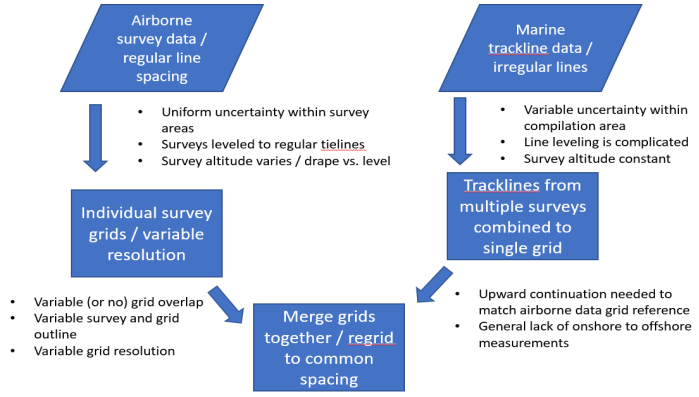

Fig. 4. Illustration of process steps and some considerations for the construction of survey-based magnetic grids.

The Australian regional map [15] is the most accurate continental scale magnetic map constructed to date.

Regional aeromagnetic compilations that are not leveled to satellite data can be digitally corrected by high-pass filtering for wavelengths less than 300 km and then adding MF7 to replace the low-passed content. An example of such a correction is shown in Fig. 5 for the Magnetic Map of East Asia [16].

Magnetic maps of marine regions are of particular interest for magnetic navigation because other alternative methods such as terrain following or image matching are not available over the oceans. These regions also present significant challenges for magnetic anomaly map preparation. For much of the open ocean the available magnetic anomaly measurements consist of marine trackline data of varying vintage, quality, and geometry. Compiling these data into trusted maps involves significant judgment and processing.

The marine regions of global magnetic anomaly maps, such as EMAG2v3 [5] and WDMAM [17] are based on the collection of marine trackline data curated and held by the National Centers for Environmental Information (NCEI), NOAA (https://www.ncei.noaa.gov/maps/geophysics/).

Fig. 6 shows a screenshot of the general availability of these data surrounding North America. The wide variation in data coverage creates challenges for consistent grid development. Some regions, mostly coastal regions in the northern hemisphere, have good data coverage at the grid spacing (for example, 4 km for EMAG2) of global compilations. Mid-ocean regions, especially in the southern hemisphere, have very sparse data coverage.

Several of the global magnetic anomaly compilations incorporate a priori information (e.g., bathymetry and/or ocean-age models) to predict and/or constrain gridding of the sparse trackline data. For example, EMAG2v2 [18] incorporates predicted anomalies based on ocean age models. EMAG2v3 [7], in contrast, does not incorporate a priori ocean age information. Incorporation of a priori information produces maps with additional information content. However, it is difficult to properly assess the reliability of the inferred anomaly features for use in alternative navigation. The range of approaches taken by available global grids indicates the need for further method development and testing.

One example of ongoing map/model development for marine regions includes an are in the north-central Caribbean [19] (Fig. 7), called the Caribbean Alt Navigation Reference Experiment (CANREx). In this study, a modern reference survey is used to validate map methodology and simultaneous cell by cell grid uncertainty estimation.

V. Alt Nav Usage

Magnetic navigation as an alternative in the absence of GPS availability has been well demonstrated in several studies, for example work by Canciani [21].

Core field magnetic models, such as the WMM and IGRF, are widely used in navigation and location applications, primarily for declination adjustment for digital compasses (or for declination notations on printed charts and maps). For example, the WMM is embedded in countless digital navigation systems and is regularly updated in these systems. These models are well calibrated and reliable. The WMM in particular, is routinely verified against independent information (as documented now annually by the NOAA/BGS "State of the Magnetic Field" reports; [22]). For "high and fast" navigation, these long-wavelength models provide excellent support for alternative navigation.

Analysis by Sandia Labs [23] concluded that the decreasing magnetic field amplitudes with altitude reduces the signal, and thus the ultimate effectiveness, for magnetic navigation. Their

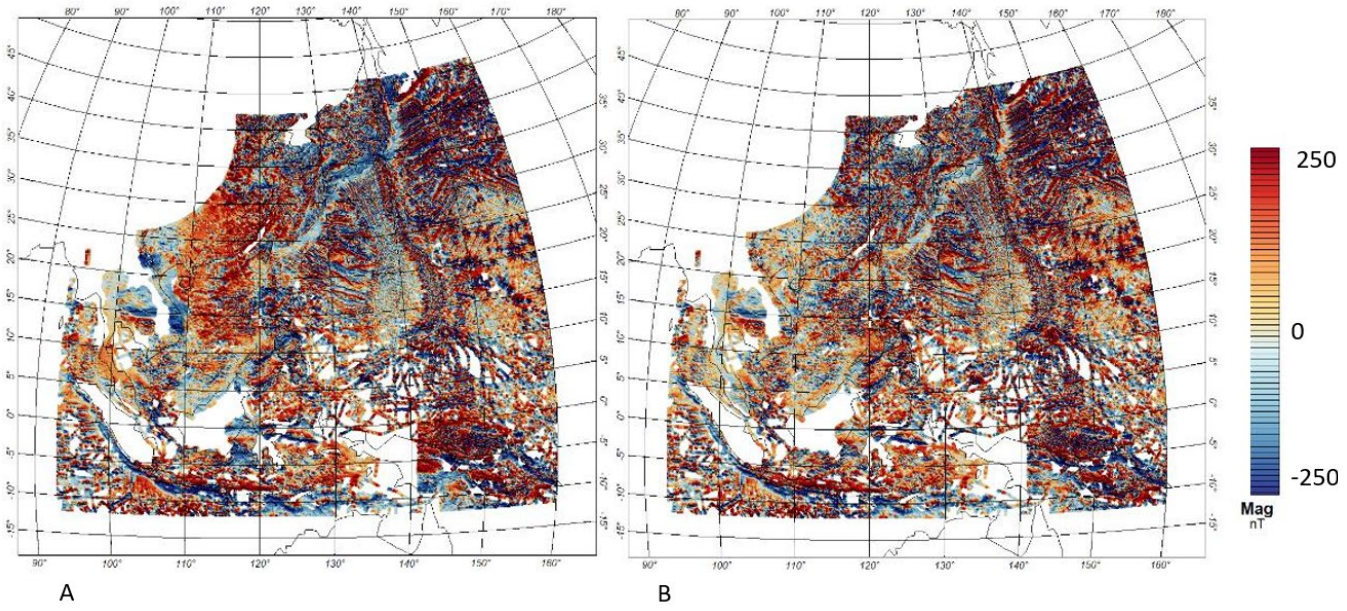

Fig. 5. Example of long-wavelength correction of a published regional magnetic anomaly map. A) Published map. B) Map with long wavelengths (>300 km) removed and replaced by MF7.

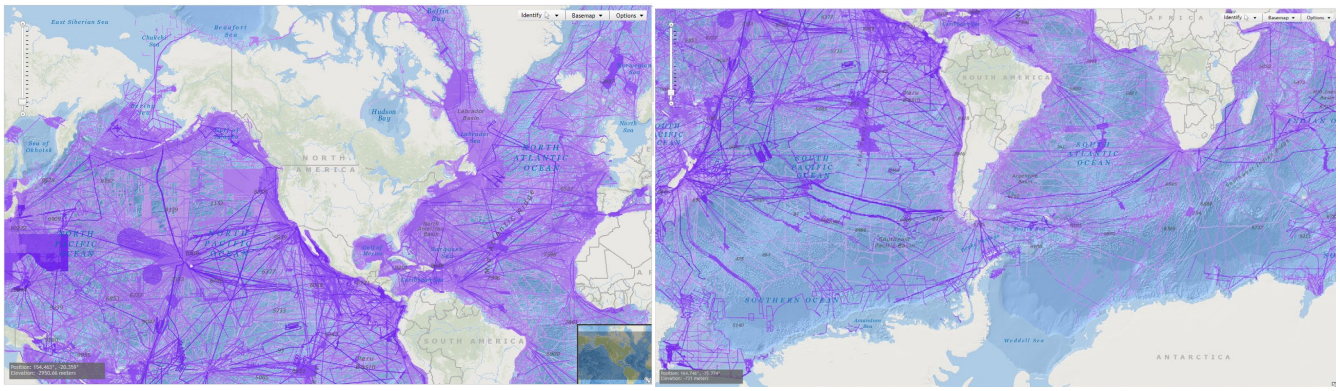

Fig. 6. General overview of available marine trackline data coverage surrounding (Left) North and (Right) South America (NCEI data portal, https://www.ncei.noaa.gov/maps/geophysics/).

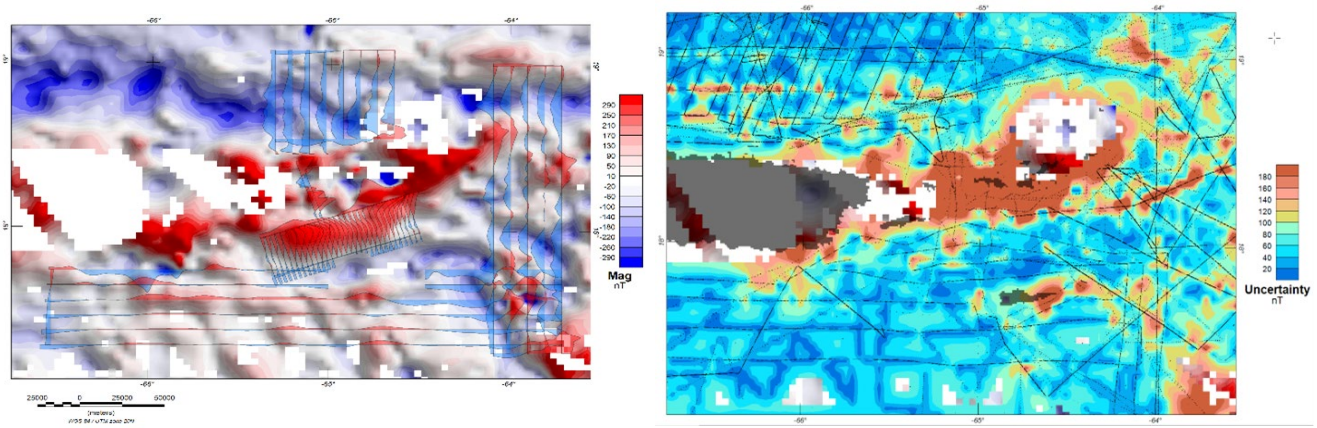

Fig. 7. Map/illustration of the CANREx study. A) Map showing magnetic anomaly values derived from trackline magnetic measurements (background colors) vs modern survey profiles (shown in profile form along survey lines). B) Map of estimated grid uncertainty based on statistical analysis of marine track line data, following [20].

study assumed no magnetic map/model uncertainty. However, magnetic map/model uncertainty is greater at low altitude than at high altitude, thus adding another factor to the analysis. Also, higher flight altitude generally correlates with higher flight velocity, further increasing the signal/time information content available to the navigator, particularly if the navigation algorithm references a core field model.

The frequency of magnetic variation of interest to the navigator varies by velocity and altitude of the moving platform. High and fast operations may require reference only to core field and large-scale lithospheric field variations. Low and slow operations are most dependent on shorter wavelengths of lithospheric anomaly maps/grids. Intermediate speed and altitude navigation requires a combination of map/model input. Evaluation of possible map/model performance for a given navigation scenario requires consideration of amplitude and frequency of magnetic field variations, magnetic map/model uncertainty, and predicted error correlation relative to the navigation path.

A simple analysis of magnetic field information versus altitude and velocity (Fig. 8 and Table 3) illustrates the interaction of these parameters for alternate navigation for two selected trajectories through the NAMAG. The top two panels in Fig. 8 show west to east profiles across portions of the lithospheric field from the North American Magnetic Anomaly Grid [2]. The top profile crosses a continental (land) area; the lower profile crosses a marine (ocean) area. Each profile is about 1000 km long. The red lines show the full resolution grid (representing a 1 km grid average values of the field at an elevation above ground of 1 km). The field is also shown as upward continued to altitudes of 5 km (green line), 10 km (black line), and 50 km (magenta line). The lower part of each profile panel shows the IGRF core field values for this profile. The IGRF total field value is a black line, and the blue line shows the IGRF plus the 50 km upward-continued lithospheric field (the magenta line in the upper panel).

Table 3 summarizes statistics on the magnetic field amplitudes and gradients for the profiles shown on Fig. 8. As the lithospheric field is upward continued from 1 to 50 km the range of anomaly amplitudes decrease: the mean absolute anomaly amplitudes and standard deviation values also decrease. Similarly, the gradient values (nT/km) decrease with altitude. The broad, high amplitude core field, in contrast, does not decrease appreciably with altitude. The result is that the steadily

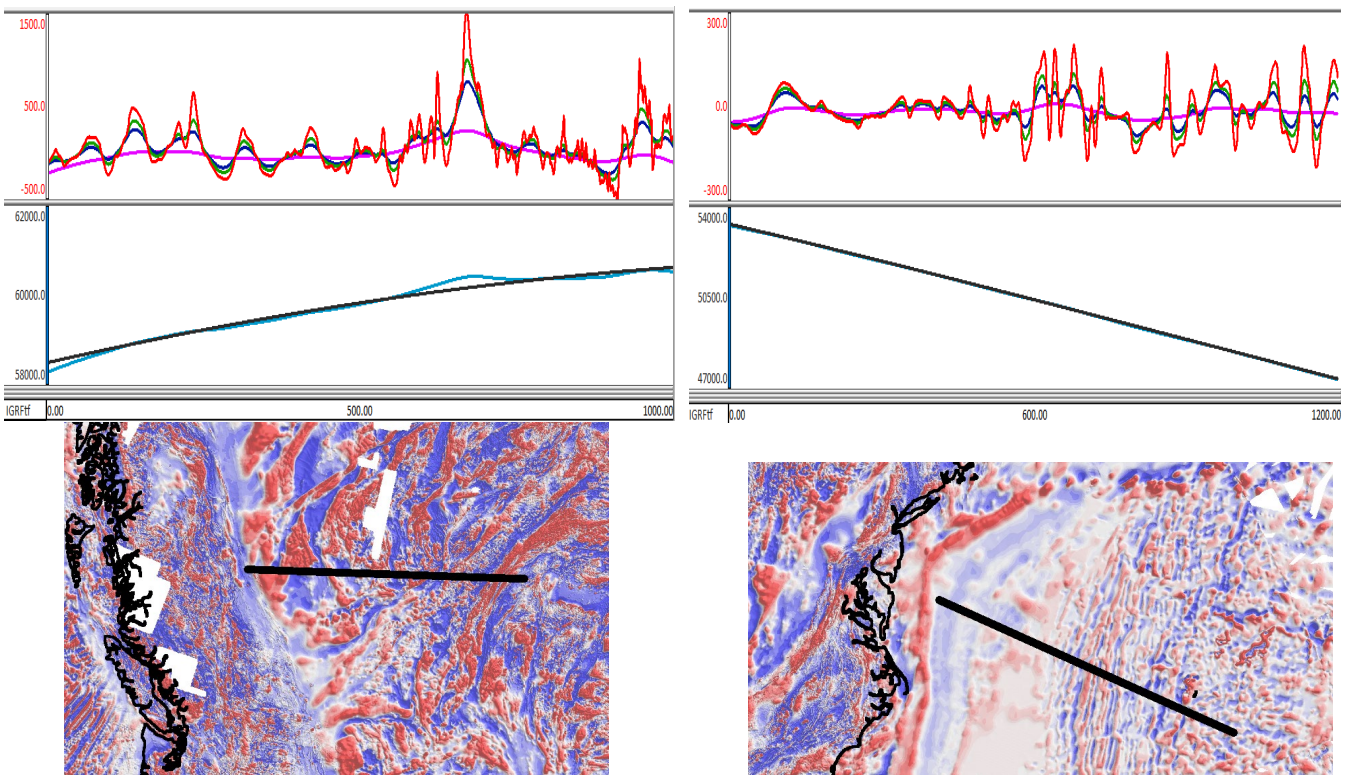

Fig. 8. Magnetic data profiles; Continental (left) and oceanic (right). Top panel: magnetic anomaly profiles along land-based track across the NAMAG (location shown below); values in nT. Red profile is the native grid data (anomaly at 1 km elevation). The green profile is data upward continued to 5 km. The dark blue profile is data upward continued to 10 km. The magenta line shows the anomalies for data upward continued to 50 km. Bottom panel: the core field (IGRF) for the same profile. The black line shows the calculated IGRF values. The cyan line shows the addition of the 50 km upward continued NAMAG anomaly (shown by the magenta line in the top panel) to the IGRF core field.

varying gradients of the core field ultimately dominate at higher altitudes. The signal (the observed time gradient of the field, nT/min) observed by a moving platform varies with altitude and velocity.

The right-hand columns of Table 3 show a simple calculation of mean anticipated signal (in units of nT/min) from lithospheric and core fields at a range of altitudes (1 to 50 km) and a range of velocities (from a slow 10 km/hr to a hypersonic 4800 km/hr). This simple calculation is a multiplication of the absolute mean gradient, times an uncertainty factor (%), times velocity. The % uncertainty value is a general approximation of expected reliability, based on the experience of our group with survey data assessment and model building of map/model gradients with altitude for continental and marine regions. This uncertainty factor represents an informed guess; formal uncertainty assessment is an on-going research activity. Despite the approximate estimate of this value, we feel it is important to include the concept of uncertainty variation with model altitude to underscore the general behavior of survey map uncertainty based on typical survey area and compilation procedures.

Taking this average time gradient of the field as a reasonable proxy for overall navigational signal, this table shows the

TABLE III. MAGNETIC FIELD STATISTICS VS ALTITUDE AND VELOCITY.

LAND	Amplitudes (nT)					Gradients (nT/km)				Uncert	Gradient Signal (nT/min) at Velocity (km/hr)					
Altitude	Min	Max	Mean	AbsMean	Stdev	Min	Max	AbsMean	Stdev	%	10 km/hr	25 km/hr	115 km/hr	170 km/hr	800 km/hr	4800 km/hr
1	-525	1517	28	192	200	-261	280	31	44	0.7	3.6	9	41.6	61.5	289.3	1736
5	-283	1010	23	144	149	-29	43	9	12	0.4	0.6	1.5	6.9	10.2	48	288
10	-215	774	18	121	124	-19	23	6	7	0.5	0.5	1.3	5.8	8.5	40	240
50	-262	245	-14	72	66	-4	2	1	2	0.6	0.1	0.3	1.2	1.7	8	48
IGRF 1 km	58519	60687	59802		635	1	3	2	1	1	0.3	0.8	3.8	5.7	26.7	160
OCEAN	Amplitudes (nT)					Gradients (nT/km)				Uncert	Gradient Signal (nT/min) at Velocity (km/hr)					
Altitude	Min	Max	Mean	AbsMean	Stdev	Min	Max	AbsMean	Stdev	%	10	25	115	170	800	4800
1	-191	198	-11	58	73	-51	43	7	11	0.5	0.6	1.5	6.7	9.9	46.7	280
5	-112	106	-12	39	46	-14	13	3	4	0.4	0.2	0.5	2.3	3.4	16	96
10	-91	67	-12	30	35	-6	7	2	2	0.5	0.2	0.4	1.9	2.8	13.3	80
50	-48	10	-16	17	13	-0.5	0.6	0.2	0.3	0.6	0	0.1	0.2	0.3	1.6	9.6
IGRF 1 km	47403	53351	50426		1728	-5.1	-4.6	5	0.2	1	0.8	2.1	9.6	14.2	66.7	400

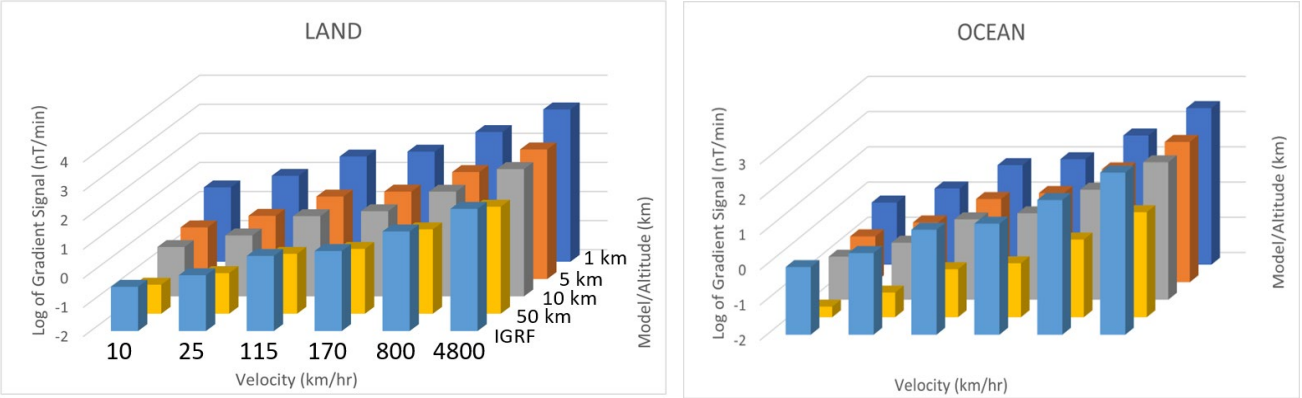

Fig. 9. Visualization of gradient signal from Table 3. (left) Gradient signal over land profile as a function of model and altitude. (right) Gradient signal over ocean profile as a function of model and altitude.

relative available navigation signal from maps/models of the lithospheric field as a trade-off of decreased signal with altitude and increased signal with velocity. If we assume that we can reliably observe nT/min gradients of 5 and above, optimum navigation potential from lithospheric field variations is achieved for the boxes colored in green in Table 3. The orange cells show suboptimal navigation signal, and the yellow boxes are nominal, perhaps requiring better sensor accuracy and calibration. Lithospheric anomaly amplitudes and gradients are generally greater over continents than over oceans, as seen in comparison of the two profiles.

The navigation potential based on reference to the long-wavelength smooth variations of the core field is relatively constant with altitude and varies primarily with velocity. Also, main field navigation requires tracking of slowly varying gradients rather than pattern matching to fluctuating gradients. Depending on the navigation algorithm used, this probably lowers, in general, the navigation potential as calculated here based mostly on the typical gradients. In any case, at some combination of increased altitude (and thus, lessened lithospheric field signal) and increased velocity (and thus greater sensing of field and gradient changes), the navigation potential of the main field exceeds that of the lithospheric field.

VI. Conclusions

In planning and development of alternative navigation systems, it is important to consider the components of the Earth's dynamic magnetic field that contribute to the measured signal for a given mission trajectory and velocity. A wide range of maps and models are available for various components of the Earth's magnetic field. It is important to select the best set for a given navigation scenario and to understand the strengths and weaknesses of the field representation.

Assessing the navigation potential for specific trajectories through survey-based lithospheric anomaly maps is a particularly challenging problem. Existing map products, particularly those developed for specific geologic or resource evaluations, may have arbitrary datums or filters applied to enhance features of interest, so that they may not be good representations of the full measured field. In addition, very few of these products include estimates of map/model uncertainty. Therefore, it is important for the makers of these models and maps to quantify the uncertainty bounds as reference for alternative navigation.

Acknowledgment

Discussions with Aaron Canciani, Aaron Nielsen, Dennis Brinkley, and others have informed and guided our research. This research was supported, in part, by the Office of Naval Research (ONR) grant N00014-20-1-2483 and by NOAA cooperative agreement NA17OAR4320101.

References

[1] A. Chulliat, W. Brown, P. Alken, C. Beggan, M. Nair, G. Cox, A. Woods, S. Macmillan, B. Meyer and M. Paniccia, The US/UK World Magnetic Model for 2020--2025: Technical Report, National Centers for Environmental Information, NOAA, doi:10.25923/ytk1-yx35, 2020.

[2] V. Bankey, A. Cuevas, D. Daniels, C.A. Finn, I. Hernandez, P. Hill, R. Kucks, W. Miles, M. Pilkington, C. Roberts, W. Roest, V. Rystrom, S. Shearer, S. Snyder, J. Velez, J. Phillips, and D. Ravat, "Digital Data Grids for the Magnetic Anomaly Map of North America," USGS Open-File Report 02-414, 2002.

[3] B. Meyer, A. Canciani, R. Saltus, and A. Chulliat, Temporal Variations of Magnetic Crustal Field Anomalies -- Implications for Source Inversion and Airborne Magnetic Anomaly Navigation, AGU Fall Meeting, 2019.

[4] B. Meyer, A. Chulliat, and R. Saltus, Derivation and Error Analysis of the Earth Magnetic Anomaly Grid at 2 arc min Resolution Version 3 (EMAG2v3), Geochemistry, Geophysics, Geosystems (AGU), 2017.

[5] Brian Meyer, Richard Saltus, and Arnaud Chulliat, EMAG2v3: Earth Magnetic Anomaly Grid (2-arc-minute resolution). Version 3. NOAA National Centers for Environmental Information, 2017.

[6] P. Alken et al., International Geomagnetic Reference Field: the thirteenth generation, Earth, Planets, Space (Springer), 10.1186/s40623-020-01288-x, 2021

[7] S. Maus, Magnetic Field Model MF7, Available at: http://geomag.org/models/MF7.html., 2010.

[8] N. Olsen, D. Ravat, C.C. Finlay, and L.K. Kother, LCS-1: A high resolution global model of the lithospheric magnetic field derived from champ and swarm satellite observations. Geophysical Journal International, 2017.

[9] C. Finlay, C. Kloss, N. Olsen, *et al.* The CHAOS-7 geomagnetic field model and observed changes in the South Atlantic Anomaly. *Earth Planets Space* 72, 156, 10.1186/s40623-020-01252-9, 2020.

[10] C. Finlay, Models of the Main Geomagnetic Field Based on Multi-satellite Magnetic Data and Gradients – Techniques and Latest Results from the Swarm Mission, Chapter 12 in M. W. Dunlop and H. Lühr (eds.), Ionospheric Multi-Spacecraft Analysis Tools, ISSI Scientific Report Series 17, 2020.

[11] A. Chulliat, A. Geomagnetic and Electromagnetic Observations at Ground Level – Geomagnetic Measurements. In M. Mandea, M. Korte, A. Yau, & E. Petrovsky (Eds.), Geomagnetism, Aeronomy and Space Weather: A Journey from the Earth's Core to the Sun (Special Publications of the International Union of Geodesy and Geophysics, pp. 54-83). Cambridge: Cambridge University Press, 2019.

[12] A. Chulliat, W. Brown, P. Alken, S. Macmillan, M. Nair, C. Beggan, A. Woods, B. Hamilton, B. Meyer and R. Redmon, Out-of-Cycle Update of the US/UK World Magnetic Model for 2015-2020: Technical Note, National Centers for Environmental Information, NOAA. doi: 10.25921/xhr3-0t19, 2019.

[13] M. Nair, A. Chulliat, A. Woods, P. Alken, and B. Meyer, "Next Generation High-Definition Geomagnetic Model for Wellbore Positioning, Incorporating New Crustal Magnetic Data," Offshore Technology Conference, OTC-31044-MS, 17 pp., 2021.

[14] C. Beggan, S. Macmillan, B. Hamilion, and W. Brown, 2019. Quantifying Uncertainties in High-resolution Magnetic Field Models. Industry Steering Committee on Wellbore Survey Accuracy (ISCWSA) 49th meeting, The Hague, Netherlands, March 8, 2019.

[15] Y. Poudjom Djomani, B. Minty, M. Hutchens, R. Lane, Total Magnetic Intensity (TMI) Grid of Australia 2019 - seventh edition - 80 m cell size. Geoscience Australia, Canberra. http://dx.doi.org/10.26186/5e9cf3f2c0f1d, eCat record number 131505, 2019.

[16] W. Doo, S. K. Hsu, and L. Armada: New magnetic anomaly map of the East Asia with some preliminary tectonic interpretations. Terr. Atmos. Ocean. Sci., 26, 73-81, doi: 10.3319/TAO.2014.08.19.07(GRT), 2015.

[17] V. Lesur, M. Hamoudi, Y. Choi, *et al.* Building the second version of the World Digital Magnetic Anomaly Map (WDMAM). *Earth Planet Sp* 68, 27. https://doi.org/10.1186/s40623-016-0404-6, 2016.

[18] S. Maus et. al. EMAG2: A 2–arc min resolution Earth Magnetic Anomaly Grid compiled from satellite, airborne, and marine magnetic measurements, Geochemistry, Geophysics, Geosystems, 2009.

[19] R. Saltus, A. Chulliat, B. Meyer, M. Bates, and A. Sirohey, Magnetic Anomaly Grid and Associated Uncertainty from Marine Trackline Data: The Caribbean Alternative Navigation Reference Experiment (CANREx), AGU Earth and Space Sci., 2023.

[20] G. Wang, M. Dai, S. Shen, Y. Bai, and Y. Xu. Quantifying uncertainty sources in the gridded data of sea surface CO2 partial pressure, J. Geophys. Res. Oceans, 119, doi:10.1002/2013JC009577, 2014.

[21] A. Canciani and J. Raquet, "Airborne Magnetic Anomaly Navigation," *IEEE Transactions on Aerospace and Electronic Systems*, vol. 53, no. 1, pp. 67–80, Feb. 2017.

[22] NCEI (U.S.), and British Geological Survey (UK), December 2022 State of the Geomagnetic Field, https://doi.org/10.25923/8r5d-fj70, December 2022.

[23] N. Claussen, L. Le, R. Ashton, K. Cespedes, A. Patel, L. Williams, B. Miller, J. Searcy, "Magnetic Navigation for GPS-Denied Airborne Applications," SANDIA REPORT SAND2020-376, 2020.